Supercapacitor Charge Redistribution Analysis for Power Management of Wireless Sensor Networks

Ruizhi Chai[1], Hanbin Ying[2], Ying Zhang[3,*]

[1]School of Electrical and Computer Engineering, Georgia Institute of Technology, Atlanta, GA, 30332 USA.
[2]School of Electrical and Computer Engineering, Georgia Institute of Technology, Atlanta, GA, 30332 USA.
[3]School of Electrical and Computer Engineering, Georgia Institute of Technology, Atlanta, GA, 30332 USA.
[*]yzhang@gatech.edu

Abstract: To support many power management applications in wireless sensor networks, a previously developed model is modified to predict the terminal behavior of a supercapacitor under a dynamic charging/discharging power profile. In addition, a robust model parameter identification method based on the Genetic algorithm is developed to determine the model parameters using a dynamic test and a self-discharge experiment. Based on the supercapacitor power input model, charge redistribution related figures of merit are derived and used to evaluate the significance of charge redistribution for supercapacitors with various rated capacitance. The results show that supercapacitors with different sizes share similar charge redistribution phenomenon. Furthermore, the charge redistribution significance is studied from several perspectives to provide guidelines for designing power management techniques that can achieve full potential of the energy stored in the supercapacitors.

1. Introduction

As a viable complement to batteries, supercapacitors, also known as ultracapacitors, or electrochemical double-layer capacitors, have a much longer lifetime with the number of charge-discharge cycles greater than $500,000$ [1]. Moreover, the supercapacitors are known to have higher power density, which allows them to output relatively large current [2]. Additional advantages include simple charging requirement and robustness to temperature changes, shock, and vibration. The main disadvantages of a supercapacitor are its low energy density, which is about one order of magnitude lower than that of batteries, and the higher leakage rate, which results in a gradual drop in supercapacitor open circuit voltage. Rechargeable batteries [3], on the other hand, feature higher energy density and lower leakage rate, but the capacity decreases with the number of charge-discharge cycles. Thus after one or two years' operation, the battery has to be replaced.

Because of its advantages, supercapacitors have been employed in various applications, such as electric, hybrid electric, and fuel cell vehicles [4, 5, 6], public transportation [7, 8], heavy machinery [9, 10], subwatt energy harvester [11], battery hybridization [12, 3, 13], etc. Researchers in the field of wireless sensor networks have also proposed using supercapacitors as energy buffers [14, 15, 16]. For wireless sensor nodes with energy harvesting capabilities, for examples solar

photovoltaic arrays [17], it is not necessary to store a large amount of energy, therefore employing supercapacitor-based energy storage systems could effectively prolong the lifetime of the sensor nodes. In most applications mentioned, the supercapacitor is plugged into a microgrid through a converter [18]. As a result, a supercapacitor behaves as either a power load (when it is charging) or a power source (when it is discharging).

In wireless sensor network applications, a supercapacitor model that can predict its terminal behavior for given load/source power profiles is important to support power management. A supercapacitor model [14], called the energy iteration equation (EIE) model, is developed based on the traditional capacitor model. In the EIE model, the relationship between the remaining energy of a supercapacitor and its leakage power is established first. Then the energy stored in the supercapacitor is predicted recursively given the power consumption and leakage power profiles. Based on this model, a leakage-aware feedback duty cycle controller is developed in [20] to maintain the energy neutral operation of sensor nodes. The EIE model only takes self-discharge into account and assumes self-discharge is the only internal energy loss. However, according to Yang [21] and Merrett [22], the terminal behavior of supercapacitor can not be modeled by conventional capacitor model because of the special porous structure of the supercapacitor electrode. As a result, charge redistribution may also have significant impact on power management.

In the work of Zhang [23], the authors propose a simple two-branch equivalent circuit model (VLR model) for wireless sensor network applications, which was shown to be able of capturing the supercapacitor behavior fairly well for given charging/discharging current profiles. It uses two RC branches to represent the intermediate and long-term behavior of supercapacitor and a large parallelly connected variable resistance to model the self-discharge of supercapacitor. In [26], a practical model is developed from the VLR model to estimate the internal state of charge redistribution process of supercapacitor. The method uses the measured terminal voltage values as input, and calculate the quickly available energy and non-quickly available energy stored in the supercapacitor, presenting a good trade-off between accuracy and simplicity.

The charge redistribution is also studied in the work of Graydon [27], which uses a two-branch equivalent circuit to model the charge redistribution and investigates an ultra-microporous aqueous electrochemical capacitor. The results indicate that on average 17.7 percent of charge are stored in the smallest pores and the resistance to ionic movement is four orders of magnitude higher than in the bulk electrolyte. The authors claim that a significant fraction of the capacitance of the electrode is not accessible during time frames of practical interest and is therefore wasted. Furthermore, a survey of the supercapacitor parameters in the literature of previous researchers indicate that the resistance ratios and capacitance ratios between that in the slow branch and that in the immediate branch are similar for various supercapacitors with organic electrolyte. However, the authors didn't provide a consistent investigation of the charge redistribution among different sizes of supercapacitor and answer the question of how to benefit from the charge redistribution in the power management applications.

To support many power management algorithms in wireless sensor networks, the model in our previous work [26] is modified to predict the supercapacitor terminal behavior using charging/discharging power profiles as input. In addition, a more robust model parameter determination method is developed based on the Genetic algorithm. Then the model is used to evaluate the significance of supercapacitor charge redistribution from three aspects. First, charge redistribution related figures of merit are derived and used to evaluate charge redistribution characteristics of supercapacitors with various rated capacitance. The results indicate that supercapacitors with different rated capacitance share similar charge redistribution phenomenon. Second, the potential

impact of charge redistribution on power management is analyzed quantitatively for supercapacitors with various rated capacitance, which provides guidelines for the design of power management techniques. Finally, a simulated system with a supercapacitor connected to a wireless sensor node via an interface circuit is studied. The results show that charge redistribution is significant under different initial conditions, and the energy loss caused by the interface circuit is negligible comparing with the energy benefit from charge redistribution. These investigations indicate that regardless of the supercapacitor size and initial condition, the charge redistribution has an important impact on power management and thus needs to be taken into account for designing power management strategies.

The remainder part of the paper is organized as follows. Following the introduction, Section 2 presents the modeling method that describes the dynamic behavior of supercapacitor fed by a dynamic charging/discharging power profile. The model parameters are then identified using genetic algorithm. The charge redistribution significance of supercapacitor with various rated capacitance is investigated in Section 3. Its potential energy benefit is studied in Section 4. Guidelines for developing energy aware power management techniques are presented based on the energy benefit analysis. At last, the paper is concluded in Section 5.

2. Supercapacitor Power Input Model for Wireless Sensor Network Applications

2.1. Dynamic power-fed supercapacitor behavior

The supercapacitor is composed of two electrodes, electrolyte, and a separator. The electrodes are usually made of porous material such as activated carbon to increase the surface area. The two porous electrodes are immersed in electrolyte and separated by porous insulating membrane. During the charging process, electrons accumulate at negative electrode. But there is no charge transfer between electrode and electrolyte. Instead, an electrochemical double-layer of charge is formed at the interface between the electrode and electrolyte. Moreover, the porous nature of supercapacitor electrode cause different charging/discharging characteristic throughout the electrode material. Because the pore size is comparable to the ion size, the limited conductance of the electrolyte leads to a voltage drop along the pore. The macro-pores get charged/discharged much more quickly than the meso- and micro-pores. Through time, the charge stored in the macro-pores migrate to the deeper pore structures. Thus the distinct terminal voltage drop in the case of short charging cycles is actually caused by both the effect of redistribution of ions to areas of low ion concentration and self discharge, which may be caused by overpotential decomposition of the electrolyte, redox-reactions due to impurities or possible internal ohmic leakage pathway of the double-layer at the electrolyte-carbon interface.

The VLR model (Fig. 1) is proposed in previous literatures [23, 24] to better capture the long-term behavior of supercapacitor. It models the charge redistribution process and self-discharge process as equivalent circuit components, which makes it straightforward to analyze the significance of charge redistribution. In this model, the input and output regulators are neglected to facilitate the analysis.

The first branch of the VLR model consists of a resistor R_1, a constant capacitor C_0 and a voltage dependent capacitor $\frac{K_v}{2} * V_1$, in which V_1 is the voltage of the first branch capacitor and $\frac{K_v}{2}$ represents the slope of the capacitance with respect to V_1. This branch is named as intermediate branch, which models the instant behavior of supercapacitor, whose capacitance increase with terminal voltage. The total capacitance of the first branch can be calculated as $C_1 = C_0 + \frac{K_v}{2} * V_1$.

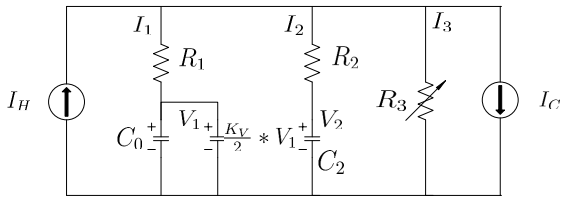

Fig. 1. *Supercapacitor VLR model with charging/discharging currents [26]*

The time constant of first branch is on the order of seconds. The second branch is composed of a resistor R_2 and a constant capacitor C_2. This branch models the charge redistribution and long-term behavior of supercapacitor with a time constant of minutes. The variable leakage resistance R_3 characterizes the time varying self-discharge.

To derive the supercapacitor model that takes power as input, the VLR equivalent circuit model is employed. According to Kirchhoff's current law, the relationship of the three branch currents can be described by

$$I_1 + I_2 + I_3 = I_H - I_C. \tag{1}$$

For the first branch, we have

$$V_t(t) = I_1(t)R_1 + V_1(t). \tag{2}$$

$$I_1(t) = [C_0 + K_V V_1(t)]\frac{dV_1(t)}{dt}. \tag{3}$$

In which, V_1 is the voltage of the first branch capacitor. The dynamics of the first branch can be represented by

$$\frac{dV_1(t)}{dt} = \frac{V_t(t) - V_1(t)}{R_1C_0 + R_1K_V V_1(t)}. \tag{4}$$

The numerical solution is solved as

$$V_1[n] = V_1[n-1] + T * \frac{V_t[n-1] - V_1[n-1]}{R_1C_0 + R_1K_V V_1[n-1]}. \tag{5}$$

Similarly, the second branch has

$$V_t(t) = I_2(t)R_2 + V_2(t), \tag{6}$$

and

$$I_2(t) = C_2\frac{dV_2(t)}{dt}. \tag{7}$$

The ordinary differential equation that describes the second branch is

$$\frac{dV_2(t)}{dt} = \frac{V_t(t) - V_2(t)}{C_2R_2} \tag{8}$$

The numerical solution is

$$V_2[n] = V_2[n-1] + \frac{T}{R_2C_2}(V_t[n-1] - V_2[n-1]). \tag{9}$$

The third branch current can be calculated as

$$I_3 = \frac{V_t}{R_3}, \tag{10}$$

in which, R_3 is a piece wise linear function of terminal voltage V_t.

The relationship between supercapacitor terminal voltage V_t and its internal state V_1 and V_2 can be derived as

$$\begin{aligned} V_t &= V_1 + I_1 R_1 = V_1 + (-I_2 - I_3 + I_H - I_C)R_1 \\ &= V_1 + (-\frac{V_t}{R_3} - \frac{V_t - V_2}{R_2})R_1 + (I_H - I_C)R_1 \\ &= V_1 - \frac{R_1}{R_3}V_t - \frac{R_1}{R_2}(V_t - V_2) + (I_H - I_C)R_1 \\ &= V_1 + \frac{R_1}{R_2}V_2 - (\frac{R_1}{R_3} + \frac{R_1}{R_2})V_t + (I_H - I_C)R_1. \end{aligned} \tag{11}$$

V_t can be calculated by

$$V_t = R_M[V_1 + \frac{R_1}{R_2}V_2 + (I_H - I_C)R_1], \tag{12}$$

where

$$R_M = \frac{R_2 R_3}{R_2 R_3 + R_1 R_2 + R_1 R_3}. \tag{13}$$

Since charging/discharging current can be represented by

$$I_H(t) - I_C(t) = \frac{P(t)}{V_t(t)}, \tag{14}$$

(12) can be translated into

$$V_t^2(t) - R_M(V_1(t) + \frac{R_1}{R_2}V_2(t))V_t(t) - R_M R_1 P(t) = 0. \tag{15}$$

The solution of (15) is

$$\begin{aligned} V_{est}(t) = &\frac{R_M}{2}(V_1(t) + \frac{R_1}{R_2}V_2(t)) \\ &+ \sqrt{\frac{1}{4}R_M^2(V_1(t) + \frac{R_1}{R_2}V_2(t))^2 + R_M R_1 P(t)}. \end{aligned} \tag{16}$$

Here, $V_t(t)$ is replaced by $V_{est}(t)$, which is used to represent the estimated terminal voltage value.

Thus, assuming the supercapacitor state (V_1 and V_2) at any time t is given, the terminal voltage of the supercapacitor V_{est} at time t can be estimated. Furthermore, the supercapacitor state at time $t + \Delta t$ can be calculated from $V_{est}(t)$ based on (5) and (9). Therefore, terminal voltage of supercapacitor can be recursively predicted as long as the power input $P[n]$ is given for each time step.

At each time slot, terminal voltage is predicted using simple mathematical operations. Therefore, the computational cost of the proposed modeling method is mainly determined by the step size, T.

What is to be noticed is that the value of R_M has to be determined before calculating the terminal voltage V_{est} as in (16). While, to calculate R_M, the value of R_3 is needed, which is a piece wise linear function of terminal voltage V_{est}. To solve this problem, the estimated terminal voltage V_{est} in the previous time slot is used to determine R_3, and then calculate for R_M. This approximation is reasonable if the step size T is not very large. As a matter of fact, the variance of R_3 has been shown to have little impact on the short-term and mid-term behavior of supercapacitor.

The model proposed in our previous work [26] estimates the supercapacitor state of charge given its terminal voltage measurement. The model developed in this paper intend to use the predicted charging power profile (for energy harvesting sensor nodes) and estimated power consumption of various tasks as input and predict the terminal voltage of supercapacitor. The purpose of the power input model is to support many power management applications in which the terminal behavior needs to be predicted based on the desired working status of of sensor node and the estimated harvesting energy. These power management algorithms often use the predicted terminal voltage to decide if the power consumption of the sensor node needs to be adjusted to maintain energy neutral operation, since the supercapacitor terminal voltage needs to be larger than a threshold to guarantee minimum operation of the sensor node.

Moreover, the model in our previous work [26] can be used in conjunction with the model developed in this paper to conduct receding horizon power management [28]. At each planning interval, the current state of charge could be estimated with the measured terminal voltage, and then used as the initial condition for predicting the terminal behavior for a finite horizon. Optimal power management strategy can be calculated for the finite horizon. Then at the next time interval, this process can be repeated to calculate the optimal strategy for the next finite horizon. With the receding horizon power management, the influence of model uncertainty and perturbation can be greatly reduced. Furthermore, the developed power input model can also be used in the simulations to study the characteristics, especially the charge redistribution, of supercapacitor fed by a dynamic charging/discharging power profile.

2.2. Model parameter identification of supercapacitor

A parameter identification method is proposed for the VLR model in the work of Yang[24]. The parameter identification procedures are based on two experiments: a charge-redistribution experiment for the first and second branches, and a self-discharge experiment for the leakage branch. The identified model parameters will then be further validated by a dynamic test, which includes several charging and discharging processes. The Maccor system [25] is used to perform the three experiments.

However, the model parameter identification method in previous work is based on three assumptions. The first assumption is that there is no interaction among branches during rapid charging or discharging, which is generally not true. The second one assumes there is no leakage during the charge redistribution experiment. But self-discharge is constantly happening as long as the terminal voltage of supercapacitor is not zero. The third assumption assumes the charge redistribution stops at $t = 3\tau_2$, in which τ_2 is the time constant of the second branch. This indicates the voltages of first branch and second branch achieve balance at time $3\tau_2$. It often requires many trial and error to find an appropriate value for $3\tau_2$. Therefore, multiple trials have to be conducted to find a good set of parameters.

To bypass the assumptions of previous work and facilitate the identification process, a genetic algorithm based identification method is presented. With the proposed method, a dynamic test is performed to identify the first and second branch parameter values and a self-discharge experiment is performed to identify the variable leakage resistance. Then a different dynamic test has to be conducted to validate the identified parameters. For differentiation purpose, the first dynamic test profile is called the training profile and the second dynamic test profile is the testing profile.

The genetic algorithm is used to find parameter values that minimizes the fitness function that will be defined later. To reduce the search space of the genetic algorithm, the following constraints are added based on the supercapacitor characteristics.

1. R_1 can be estimated given the ESR value from the data sheet. The constraint for R_1 is
$$R_1 \in [ESR - \delta_1, ESR + \delta_1], \tag{17}$$
in which, δ_1 can be chosen as $\delta_1 = 0.02 * ESR$. This is based on the fact that R_1 is very similar compared to the value of ESR.

2. The constraint for the first branch capacitance is
$$C_0 < C_{rated} \tag{18}$$
and
$$C_0 + \frac{K_v}{2} \times V_{rated} + C_2 > C_{rated}. \tag{19}$$
This is because C_0 corresponds to the minimum capacitance and $C_0 + K_v \times V_{rated} + C2$ corresponds to the maximum capacitance of supercapacitor. The capacitance range of supercapacitor must contains the rated capacitance.

3. The constraint for second branch capacitance is
$$C_2 < C_0. \tag{20}$$
This constraint is due to the fact that the redistributed charge is only a small portion of the total charge. Because of the finite conductance of electrolyte and the small size of micro and meso pores, charge stored in these pores are limited. Therefore, C_2, which represents the storing capacity of these pores, must be smaller than C_0.

4. The time constants of first and second branches must satisfy
$$\frac{(C_0 + K_v \times V_1)R_1}{C_2 R_2} < 0.01. \tag{21}$$
This constraint is used to make sure the ratio of first and second branch time constant is smaller than 0.01, thus the two branches represent the immediate dynamic and delayed dynamic of supercapacitor respectively.

The optimization problem can be formulated as

$$\begin{aligned} \underset{X}{\text{minimize}} \quad & \text{fitness}(X) \\ \text{subject to} \quad & C_0 < C_{rated}, \\ & C_0 + \frac{K_v}{2} \times V_{rated} + C_2 > C_{rated}, \\ & C_2 < C_0, \\ & \frac{(C_0 + K_v * V_1) * R_1}{C_2 R_2} < 0.01. \end{aligned} \tag{22}$$

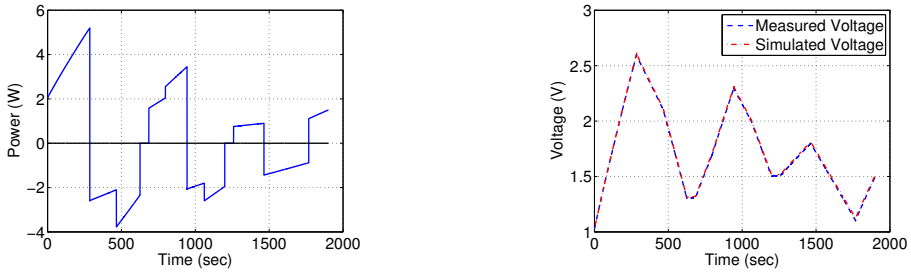

(a) (b)

Fig. 2. *(a) Training power profile. (b) Comparison between measured and simulated voltages.*

In (22), X is a vector that represents the set of parameters $(R_1, R_2, C_0, K_v, C_2)$. $\text{fitness}(X)$ represents the squared error between the measured voltage and the voltage estimated by the model using the parameter set X.

A 310 F 2.7 V supercapacitor is used to validate both the parameter identification method and the supercapacitor power input model. The dynamic charging/discharging power profile used for training is shown in Fig. 2(a). Before the experiment, the supercapacitor is charged by a 1 volt constant voltage source for an hour, therefore the initial values of V_1 and V_2 are 1 V. The terminal voltage of supercapacitor during the test is measured and shown in Fig. 2(b).

Since the genetic algorithm is a random search algorithm in nature, we run the genetic algorithm for 25 times. For each run, the population of each generation is 500. The maximum number of generations can be 200. But the algorithm will be terminated if the fitness value no longer shows improvement. The set of parameters corresponding to the smallest fitness value is selected as the parameter for the 310 F 2.7 V supercapacitor, which is shown in Table 1. The voltage simulated by the power input model is compared with the measured data as in Fig. 2(b), which indicates that the identified model parameters can represent the terminal behavior of the supercapacitor.

Table 1 Model Parameter of a 310 F 2.7 V Supercapacitor

$R_1(Ohm)$	$R_2(Ohm)$	$C_0(Farad)$	K_V	$C_2(Farad)$
0.00224	10	298.37960	29.994	12.077

After determining the parameters of first and second branches, the value of variable resistor R_3 is related to the terminal voltage V_{term} by a piecewise linear function as in (23).

$$R_3 = \begin{cases} (-3190) * V_{term} + 8831 \\ \qquad \text{if } V_{term} \in [2.628, 2.7) \\ (-6342) * V_{term} + 1.711 \times 10^4 \\ \qquad \text{if } V_{term} \in [2.574, 2.628) \\ (-1.044 \times 10^4) * V_{term} + 2.766 \times 10^4 \\ \qquad \text{if } V_{term} \in [2.552, 2.574) \\ (-1.683 \times 10^4) * V_{term} + 4.387 \times 10^4 \\ \qquad \text{if } V_{term} \in [2.488, 2.552) \\ (-4.773 \times 10^4) * V_{term} + 1.202 \times 10^5 \\ \qquad \text{if } V_{term} \in [2.379, 2.488) \\ (-2.082 \times 10^5) * V_{term} + 5.009 \times 10^5 \\ \qquad \text{if } V_{term} \in [0, 2.379) \end{cases} \tag{23}$$

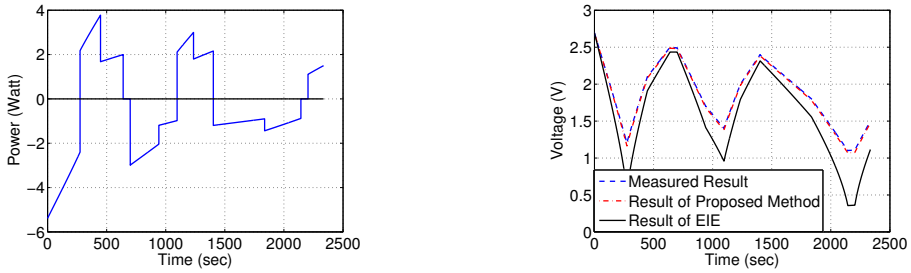

(a) (b)

Fig. 3. *(a) Testing power profile. (b) Comparison between measured and simulated voltages.*

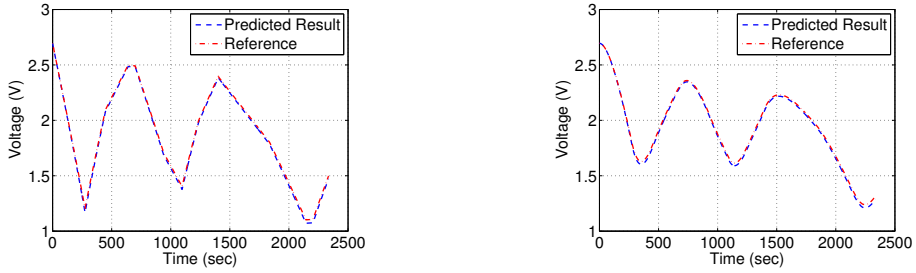

(a) (b)

Fig. 4. *(a) V_1 comparison. (b) V_2 comparison.*

The identified model parameters are validated using a testing power profile as in Fig. 3(a). The initial state of the supercapacitor is $V_t = V_1 = V_2 = 2.7V$. This is achieved by charging the supercapacitor with a 2.7 V constant voltage source for one hour before the dynamic test. The comparison of the simulated voltage and the measured voltage is shown in Fig. 3(b). It is shown that the terminal behavior of supercapacitor can be accurately predicted by the developed power input model with the identified parameters. For comparison, the supercapacitor terminal behavior predicted by the EIE model is also shown in Fig. 3(b). EIE model significantly underestimate the terminal voltage since the charge redistribution phenomenon is neglected. Moreover, the internal state of supercapacitor is estimated from the measured terminal voltage using the numerical method proposed in previous literature [26]. The internal state variables (V_1 and V_2) are then compared with that estimated from the method in Section 2.1. The results are shown in Figure 4. It indicate that the internal states can also be captured by the proposed modeling method. In the following sections, this model will be used to analyze the influence of charge redistribution on power management.

3. Influence of Rated Capacitance on Charge Redistribution Significance

3.1. Figures of merit for charge redistribution

Based on the developed model, two figures of merit can be defined for evaluating charge redistribution in supercapacitor. To derive the figures of merit, we first calculate the currents that flow into the two branches, since the currents of immediate branch and delayed branch represent the speed of charge accumulation in the two branches.

According to (2) and (6), the relation between the first branch current I_1 and the second branch current I_2 can be derived as:

$$I_1 = \frac{V_t - V_1}{R_1} = \frac{I_2 R_2 + V_2 - V_1}{R_1} = I_2 \frac{R_2}{R_1} - \frac{V_1 - V_2}{R_1}. \tag{24}$$

Plug (24) into (1) gives:

$$(\frac{R_2}{R_1} + 1) I_2 - \frac{V_1 - V_2}{R_1} = I_H - I_C - I_3. \tag{25}$$

Thus, I_2 can be solved as

$$I_2 = \frac{R_1}{R_1 + R_2}(I_H - I_C - I_3) + \frac{V_1 - V_2}{R_1 + R_2}, \tag{26}$$

and I_1 can be solved using the similar way as

$$I_1 = \frac{R_2}{R_1 + R_2}(I_H - I_C - I_3) - \frac{V_1 - V_2}{R_1 + R_2}. \tag{27}$$

Equation (26) and (27) show that the currents injected into the first and second branch are composed of two components. The first one is the result of charging/discharging current minus the self-discharge current. The second one is caused by the charge redistribution effect. For example, on the right hand side of (26), the first term is the result of external charging/discharging, and the second term is the result of charge redistribution. When $V_1 > V_2$, the charge transfers from first branch to second branch, which makes the second term positive. While when $V_1 < V_2$, charge transfers from second branch back to first branch. And the second term becomes negative.

Let

$$K_c = \frac{R_2}{R_1 + R_2}, \tag{28}$$

then

$$1 - K_c = \frac{R_1}{R_1 + R_2}. \tag{29}$$

K_c represents the portion of charge injected into the first branch. Larger K_c means more charge flow into the first branch and less charge flow into the second branch. This causes the unbalance of charge storage in the first two branches.

From the second term on the right hand side of (26) and (27), the second charge redistribution related figure of merit can be derived. It reflects the charge transfer between the first two branches. As is shown, the redistribution current depends on $|V_1 - V_2|$. Moreover, the the redistribution current is monotonically decreasing, since the value of $|V_1 - V_2|$ is decreasing. Therefore, the decreasing rate of $|V_1 - V_2|$ can reflect the significance of charge redistribution.

The dynamic change of $V_1 - V_2$ is analyzed as follows with two assumptions. First, assume there is no external charging or discharging to focus on redistribution between the first two branches. Second, the effect of self-discharge is neglected because of the small magnitude of self-discharge current. With these assumptions, first branch dynamic can be represented by

$$\frac{V_2 - V_1}{R_1 + R_2} = (C_0 + K_v V_1) \frac{dV_1}{dt}, \tag{30}$$

and the second branch dynamic can be described as

$$\frac{V_1 - V_2}{R_1 + R_2} = C_2 \frac{dV_2}{dt}. \tag{31}$$

Thus the dynamic of $V_1 - V_2$ can be derived as

$$\begin{aligned} \frac{d(V_1 - V_2)}{dt} &= \frac{dV_1}{dt} - \frac{dV_2}{dt} \\ &= \frac{V_2 - V_1}{(R_1 + R_2)(C_0 + K_v V_1)} + \frac{V_2 - V_1}{(R_1 + R_2)C_2} \\ &= \frac{V_2 - V_1}{R_1 + R_2}\left(\frac{1}{C_0 + K_v V_1} + \frac{1}{C_2}\right). \end{aligned} \tag{32}$$

Let

$$K_r = \frac{1}{R_1 + R_2}\left(\frac{1}{C_0 + K_v V_1} + \frac{1}{C_2}\right), \tag{33}$$

then (32) can be converted to

$$\frac{d(V_1 - V_2)}{dt} = -K_r(V_1 - V_2). \tag{34}$$

If K_r was a constant, the solution of $V_1(t) - V_2(t)$ is

$$V_1(t) - V_2(t) = [V_1(0) - V_2(0)]e^{-K_r t}, \tag{35}$$

where K_r represents the rate of decay of $V_1(t) - V_2(t)$. Here, K_r is a function of V_1, which is not a constant. The value of V_1 changes within $[1.0, 2.7]$, since in practice a DC-DC converter is often used to stabilize the output voltage of the supercapacitor, which has a minimum input voltage of 1 volt. Although K_r is not a constant, it still represents the rate of balancing of two branch capacitors, which also reflects the significance of charge redistribution.

In summary, the significance of charge redistribution can be described by K_c and K_r. K_c represents the portion of current injected into or extracted from the first and second branches. It reflects the significance of charge redistribution from the charge accumulation or extraction point of view. K_r represents the rate of balancing of $V_1(t)$ and $V_2(t)$, which reflects the significance of charge redistribution from the internal charge balancing point of view. In the next section, it will be shown that for supercapacitors with different rated capacitance, K_c and K_r have similar values. Thus different types of supercapacitors share similar charge redistribution phenomenon.

3.2. Charge Redistribution Analysis of Supercapacitors with Different Rated Capacitance

In this section, the charge redistribution phenomenon of supercapacitors with various rated capacitance are studied based on the proposed figures of merit. The investigated supercapacitors are manufactured by Maxwell with a rated capacitance of 5 F, 10 F, 50 F, 100 F, 150 F and 310 F.

The parameter identification method proposed in Section 2.2 is employed to identify the parameters for all the supercapacitors. Since the parameters can be different even for supercapacitors with the same rated capacitance due to the manufacture process, two samples are tested for each

type of supercapacitor (three samples for 5 F supercapacitor), and the average value of the parameters are calculated to reveal the common feature for the type of supercapacitor. Using the average values, K_c and K_r are calculated to evaluate the significance of charge redistribution for the corresponding type of supercapacitor. What is to be noticed is that, K_r depends on the value of V_1. Thus three K_r are calculated. Max K_r represents the value corresponding to $V_1 = 1$ V. Min K_r corresponds to $V_1 = 2.7$ V. Avg K_r is calculated when $V_1 = 1.85$ V, which is the median of V_1's working region. The results are shown in Table 2.

Table 2. *Charge Redistribution Analysis of Different Type of Supercapacitor*

Supercapacitor Model	R_1	R_2	C_0	K_v	C_2	K_c	Max K_r	Avg K_r	Min K_r
5 F 2.7 V 1	0.17307	393	3.48084	1.18291	1.23364				
5 F 2.7 V 2	0.17193	229	3.97187	1.00311	1.66992				
5 F 2.7 V 3	0.17205	109	4.86758	0.56987	2.51478				
Average	0.17235	243.66667	4.10676	0.91863	1.80611	0.99929	0.00309	0.00298	0.00289
10 F 2.7 V 1	0.07593	73	7.64376	1.51538	2.16922				
10 F 2.7 V 2	0.07374	68	5.80484	2.16775	1.26870				
Average	0.07488	69.5	6.58441	1.90187	1.74104	0.99894	0.00990	0.00964	0.00945
50 F 2.7 V 1	0.02029	20	46.11091	4.84665	17.34194				
50 F 2.7 V 2	0.02040	54	47.98547	3.60377	11.43605				
Average	0.02034	37	47.04819	4.22521	14.38900	0.99945	0.00240	0.00237	0.00234
100 F 2.7 V 1	0.01484	14	82.29080	15.56573	22.99865				
100 F 2.7 V 2	0.01494	42	73.40343	19.14485	4.45104				
Average	0.01489	28	77.84712	17.35529	13.72485	0.99947	0.00298	0.00293	0.00289
150 F 2.7 V 1	0.01411	19	98.29125	29.64278	19.71274				
150 F 2.7 V 2	0.01423	19	101.09580	27.62440	13.20188				
Average	0.01417	19	99.69353	28.63359	16.45731	0.99925	0.00361	0.00354	0.00349
310 F 2.7 V 1	0.00224	10	298.37960	29.99440	12.07665				
310 F 2.7 V 2	0.00247	7	309.96540	29.96536	99.78468				
Average	0.00236	8.5	304.17250	29.97988	55.93067	0.99972	0.00245	0.00243	0.00241

From Table 2, it is obvious that even the same type of supercapacitors can have different parameters, especially for the 5 F 2.7 V supercapacitors, whose R_2 value shows notable difference. Therefore, three samples are picked for the 5 F 2.7 V supercapacitor. This phenomenon may be due to the difference in the manufacture process.

With the increase of supercapacitor rated capacitance, the value of R_1 decreases, so does the value of R_2. The values of C_0 and K_v increases. This indicates the resistance of charge transfer decreases with the increasing of supercapacitor size, and the capacitance of the immediate branch increases with the supercapacitor size. For the delayed branch, the change of capacitance is more complicated.

It is shown that the value of K_c is very similar among different types of supercapacitors. Therefore, different types of supercapacitors share the similar charging/discharging characteristics. Although the variation of the K_r value is slightly larger, they still show similar rate of balancing effect between two branches among different size of supercapacitors. In general, the results indicate that the significance of charge redistribution phenomenon is similar among different size of supercapacitors.

However, it is to be noticed that the K_c value of 10 F supercapacitor is slightly smaller and the K_r value is larger. This indicates the charge redistribution phenomenon of the supercapacitors are less significant. This may be the result of previous extensive use of the 10 F 2.7 V supercapacitors. It is known that the long-term use could cause modification of the electrode structures

and, particularly, a change in pore sizes and distribution [30]. Specifically, the diameters of the pores and the pore depth decrease with time. This is due to the impurities settlement around the wall of pores which reduces the surface area of activated carbon. Though the large pores can still accommodate electrons after power cyclings, many small pores are blocked or become too narrow for electrons. As a consequence, charge redistribution phenomenon become less significant since the storage capacity of the meso and micro pores decreases.

4. Significance of Charge Redistribution on Power Management

In this section, charge redistribution significance is studied by quantitatively estimating the energy benefit that may be achieved when $V_2 > V_1$, which is the energy redistributed to the immediate branch from the slow branch and become quickly available for task execution. Several factors that may influence the energy benefit are studied. By quantitatively estimating the energy benefit with these factors, guidelines are presented for designing the power management techniques to fully retrieve the stored energy.

4.1. Energy Benefit for Supercapacitors with Different Rated Capacitance

Since K_r represents the balancing rate between the immediate branch and the redistribution branch of a supercapacitor, it can be used to quickly estimate potential redistribution energy benefit with time for a given initial state of charge.

Although, K_r is a variable that depends on V_1 according to (33), we choose the average value in Table 2 to simplify the procedure of analysis. This is reasonable since Table 2 shows that the value of K_r doesn't change significantly. At the same time, C_1 is also treated as a constant with a value calculated at the median of the V_1's working range, $V_1 = 1.85\ V$.

Since the resistance of the third branch is very large, the charge dissipated due to leakage can be neglected. Thus

$$C_1(V_1(t) - V_1(0)) = -C_2(V_2(t) - V_2(0)). \tag{36}$$

The value of $V_2(t)$ can be represented by

$$V_2(t) = -\frac{C_1}{C_2}(V_1(t) - V_1(0)) + V_2(0). \tag{37}$$

Plug (37) into (35) gives

$$V_1(t) = \frac{C_2}{C_1 + C_2}[V_1(0) - V_2(0)](e^{-K_r t} - 1) + V_1(0). \tag{38}$$

Based on (38), if there is no external charging or discharging, the value of V_1 can be estimated given the time t and the initial state $V_1(0)$ and $V_2(0)$. Then the change of quickly available energy can be calculated as

$$\Delta E_{QA}(t) = \frac{1}{2}C_0 V_1^2(t) + \frac{1}{3}K_V V_1^3(t) - \frac{1}{2}C_0 V_1^2(0) - \frac{1}{3}K_V V_1^3(0). \tag{39}$$

The value of $\Delta E_{QA}(t)$ can be used to represent the energy benefit.

A typical case when $V_1(0) = 1.7$ V and $V_2(0) = 2$ V is taken as an example here to illustrate the energy benefit of charge redistribution for supercapacitors with rated capacitance of $5\ F$, 10

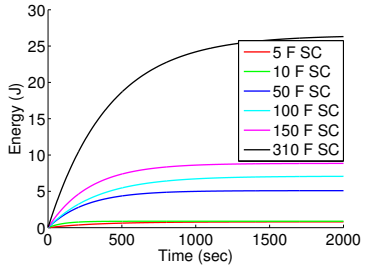

Fig. 5. *Energy Benefit of Charge Redistribution*

F, 50 F, 100 F, 150 F, and 310 F. The results in Fig. 5 show that the quickly available energy increases with time and the increase becomes less and less significant. Larger size of supercapacitors are shown to have more energy benefit than smaller size of supercapacitors for the same initial state of charge. For example, when $t = 120$ seconds, the energy benefit of 10 F supercapacitor is 0.5116 J, and the energy benefit of 310 F supercapacitor is 6.1867 J. Therefore, in real applications, depending on the power consumption of the task and the size of supercapacitor, the charge redistribution may need to be taken into account. If the energy benefit are comparable to the energy consumption of the task , then by predicting the energy benefit from charge redistribution, the task can be preassigned to fully retrieve the stored energy. Another factor that influence the energy benefit of charge redistribution is time. From Fig. 5, it is shown that charge redistribution generally has a time scale of several minutes, the benefit of predicting charge redistribution energy and making use of it may be negligible if the time scale of power management is too small.

4.2. Energy Benefit for Supercapacitors in A Practical Case

The significance of supercapacitor charge redistribution has been evaluated for different sizes with a fixed initial condition in the previous section. However, when used in the real sensor nodes, state of charge of a supercapacitor may vary a lot. In this part, the change of charge redistribution benefit with the initial condition is investigated. In addition, a DC-DC converter is always used to stabilize the varying output voltage of a supercapacitor. The DC-DC converter has additional energy loss. We will investigate if this energy loss may cancel the supercapacitor redistribution benefit.

The model parameters of the identified 310 F 2.7 V supercapacitor sample in Table 1 is used for investigation in this section. The supercapacitor is connected to a sensor node via the DC-DC converter, as shown in Fig. 6. A duty cycling scenario is created with a sleep mode lasting 120 seconds after an active mode that is assumed to create various initial state of charge for the supercapacitor.

Based on the data of the TmoteSky MICAz sensor node [33], the current consumption of sensor node during sleep mode is assumed to be $I_n = 0.0001$ Amps as a pessimistic estimation. The voltage of the sensor node is $V_n = 3.3$ V. Thus the power consumption during sleep mode can be calculated as $P_{out} = V_n \times I_n$. The duration of the sleep mode is assumed to be 120 seconds.

In previous works [19, 29], the efficiency of the DC-DC converters is assumed to be constant. However, in practice, this problem might need to be analyzed case by case. The TPS61221 DC-DC buck-boost converter from Texas Instruments [31] is used for analysis in this section. It ensures a stable and constant supply voltage of 3.3 V. The converter starts converting at an input voltage of

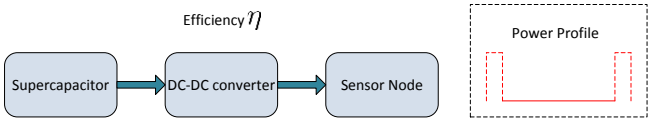

Fig. 6. *Simplified scheme of the energy storage system*

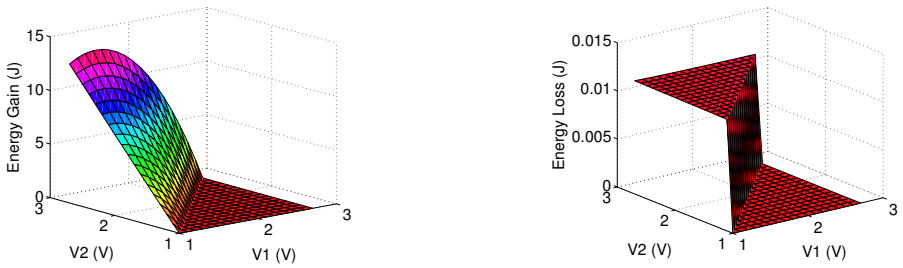

(a) (b)

Fig. 7. *(a) Energy gain due to charge redistribution. (b) Additional energy loss when the efficiency variation of DC-DC converter is considered.*

0.7 V. However, the threshold of supercapacitor terminal voltage used by sensor node is often set to be 1 V to ensure enough margin. The efficiency of the interface circuit is first assumed to be 80%.

The initial state of supercapacitor at the beginning of the sleep mode covers all the cases in $(V_1, V_2) \in [1.0, 2.7] \times [1.0, 2.7]$ that satisfies $V_2 > V_1$. Supercapacitor power input model derived in Section 2 is employed here to simulate the internal behavior of the supercapacitor and calculate the energy benefit, which is the increased energy in the first branch during sleep mode, as in (40).

$$\begin{aligned} E_{benefit} = &\frac{1}{2}C_0V_1^2(t=120) + \frac{1}{3}K_VV_1^3(t=120) \\ &-\frac{1}{2}C_0V_1^2(t=0) - \frac{1}{3}K_VV_1^3(t=0). \end{aligned} \tag{40}$$

The energy benefit can also be represented as

$$E_{benefit} = E_{redistributed} - E_{loss} - E_{sleep}, \tag{41}$$

in which, $E_{redistributed}$ denotes the redistributed energy from second branch to first branch, E_{loss} represents the energy loss due to interface circuit and E_{sleep} is the energy consumption of the sensor node during sleep mode. If $E_{benefit} > 0$, then the energy gain from redistribution is greater than the overall energy dissipation during sleep mode. Otherwise, the energy gain is canceled out by the energy loss during sleep mode.

Fig. 7(a) is the calculated energy gain at the end of sleep mode. It is shown that for all the supercapacitor states that satisfies $V_2 > V_1$ the energy gain is greater than zero. Thus the energy gain is greater than the dissipated energy during the sleep mode. Furthermore, the energy benefit from charge redistribution can be quite significant. The maximum energy benefit is as large as

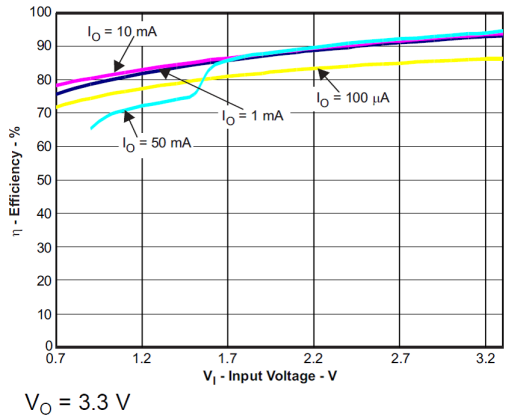

Fig. 8. *Efficiency versus input voltage and output current of the TPS61221 [31]*

13.78 Joules when $V_2 = 2.7$ V and $V_1 = 1.3$ V. When $V_2 = 2$ V and $V_1 = 1.7$ V, the energy benefit is 3.791 Joules, which is able to support radio listening task for 78 seconds according to the data of real system [32]. Thus due to the low power nature of wireless sensor network, the charge redistribution can have a significant influence on power management. The energy loss caused by DC-DC converter is $0.0099\ J$.

The previous conclusion is based on the assumption that efficiency of the interface circuit is constant. However, in real system, the decrease of efficiency when input voltage is low may lead to additional energy loss, which may eventually cancel out the benefit of charge redistribution. Therefore, the varying efficiency of DC-DC converter is taken into consideration in the simulation. According to the datasheet, the efficiency of TPS61221 can be represented as a function of supercapacitor terminal voltage and the output current as in Fig. 8. The curve of efficiency is approximated using a piece wise linear function in our investigation. Then supercapacitor is simulated using the power model and the energy gain is calculated with (40). The result is very similar with Fig. 7(a), and the difference between these two results is plotted in Fig. 7(b), which corresponds to the energy loss due to varying efficiency of DC-DC converter. It is clear that the energy loss is insignificant compared to the energy gain from redistribution. Thus the charge redistribution is significant to power management even when the varying efficiency of DC-DC converter is taken into consideration.

5. Conclusion

Supercapacitors have been employed in various applications. In most of these applications, the supercapacitor is connected to the system via an interface circuit, which is characterized by a variable energy conversion efficiency. Thus a model that describes the dynamic behavior of supercapacitor fed by a dynamic charging/discharging power profile is important for developing power management techniques. In this paper, a supercapacitor power input model is derived based on the previously developed supercapacitor practical model. The model iteratively predict the terminal voltage given the supercapacitor internal states and the charging/discharging power. Moreover, a genetic algorithm-based method is developed to facilitate the model parameter identification of supercapacitors.

Two figures of merit are derived from the power input model to evaluate the significance of charge redistribution in supercapacitors, and are used to analyze charge redistribution of supercapacitors with various rated capacitance. The results show that supercapacitors with different rated capacitance share similar charge redistribution phenomenon. Furthermore, the charge redistribution significance is studied from the perspective of power management by estimating the potential energy benefit. A method to quickly predict the available redistribution energy benefit of a supercapacitor at different time is developed based on a figure-of-merit parameter, and the potential energy benefits of supercapacitors of various sizes are analyzed using this method. The results can be used to quickly estimate whether the redistribution energy benefit is significant for a given application. In addition, the impact of charge redistribution on power management is also analyzed when the supercapacitor is connected to a sensor node via an interface circuit. The charge redistribution is still significant when taking the interface circuit efficiency into consideration. This paper indicates that charge redistribution is significant for many practical applications, and it could bring potential benefit to wireless sensor network applciations when the power management strategies are designed properly.

6. Acknowledgment

This research was supported in part by the National Science Foundation under Grant CNS-1253390.

7. References

[1] F. Simjee and P. H. Chou, "Everlast: long-life, supercapacitor-operated wireless sensor node," *Proceedings of the 2006 International Symposium on Low Power Electronics and Design (ISLPED)*, pp.197-202, 2006.

[2] R. Kötz, and M. Carlen, "Principles and applications of electrochemical capacitors," *Electrochimica Acta*, vol.45, no.15, pp.2483-2498, 2000.

[3] T. T. N. Nguyen, H. G. Yoo, S. K. Oruganti, F. Bien, "Neuro-fuzzy controller for battery equalisation in serially connected lithium battery pack," *IET Power Electronics*, vol.8, no.3, pp.458-466, 2015.

[4] A. Burke, "Batteries and ultracapacitors for electric, hybrid and fuel cell vehicles," *Proceedings of the IEEE*, vol.95, no.4, pp.806-820, 2007.

[5] J. M. Blanes, R. Gutierrez, A. Garrigos, J. L. Lizan, and J. M. Guadrado, "Electric vehicle battery life extension using ultracapacitors and an FPGA controlled interleaved buck-boost converter," *IEEE Transaction on Power Electronics*, vol.28, no.22, pp.5940-5948, 2013.

[6] O. Ladin, M. Moshirvaziri, and O. Trescases, "Predictive algorithm for optimizing power flow in hybrid ultracapacitor/battery storage systems for light electric vehicles," *IEEE Transaction on Power Electronics*, vol.20, no.8, pp.3882-3895, 2013.

[7] A. Allegre, A. Bouscayrol, P. Delarue, P. Barrade, E. Chattot, and S. El Fassi, "Energy storage system with supercapacitor for an innovative subway," *IEEE Transaction on Industrial Electronics*, vol.57, no.12, pp.4001-4012, 2012.

[8] D. Iannuzzi and P. Tricoli, "Speed-based state-of-charge tracking control for metro trains with onboard supercapacitors," *IEEE Transaction on Power Electronics*, vol.27, no.4, pp.2129-2140, 2012.

[9] S. Min and S. Sul, "Control of rubber tyred gantry crane with energy storage based on supercapacitor bank," *IEEE Transaction on Power Electronics*, vol.21, no.5, pp.1420-1427, 2006.

[10] T. Kwon, S. Lee, S. Sul, *et al.*, "Power control algorithm for hybrid excavator with supercapacitor", *IEEE Transaction on Industrial Application*, vol.46, no.4, pp.1447-1455, 2010.

[11] S. Kim, and P. H. Chou, "Size and topology optimization for supercapacitor-based sub-watt energy harvesters," *IEEE Transactions on Power Electronics*, vol.28, no.4, pp.2068-2080, 2013.

[12] I. Aharon, and A. Kuperman, "Topological overview of powertrains for battery-powered vehicles with range extenders," *IEEE Transactions on Power Electronics*, vol.26, no.3, pp.868-876, 2011.

[13] B. Hredzak, V. G. Agelidis, and M. Jang, "A model predictive control system for a hybrid battery-ultracapacitor power source," *IEEE Transactions on Power Electronics*, vol.29, no.3, pp.1469-1479, 2014.

[14] T. Zhu, Z. Zhong, Y. Gu, T. He, and Z.L. Zhang, "Leakage-aware energy synchronization for wireless sensor networks," *Proceedings of the 7th international conference on Mobile systems, applications, and services*, pp.319-332, 2009.

[15] F. Ongaro, S. Saggini, and P. Mattavelli, "Li-ion battery-supercapacitor hybrid storage system for a long lifetime, photovoltaic-based wireless sensor network," *IEEE Transactions on Power Electronics*, vol.27, no.9, pp.3944-3952, 2012.

[16] Q. Ju, and Y. Zhang, "Charge Redistribution-Aware Power Management for Supercapacitor-Operated Wireless Sensor Networks," *IEEE Sensors Journal*, vol.16, no.7, pp.2046-2054, 2016.

[17] J. D. Bastidas-Rodriguez, E. Franco, G. Petrone, C. Andres Ramos-Paja, and G. Spagnuolo, "Maximum power point tracking architectures for photovoltaic systems in mismatching conditions: a review," *IET Power Electronics*, vol.7, no.6, 1396-1413, 2014.

[18] D. Sha, and J. Chen, "Bidirectional three-phase high-frequency ac link dcac converter used for energy storage," *IET Power Electronics*, vol.8, no.12, pp.2529-2536, 2015.

[19] C. Renner, and V. Turau, "CapLibrate: self-calibration of an energy harvesting power supply with supercapacitors," *23rd International Conference on Architecture of Computing Systems*, pp.1-10, 2010.

[20] T. Zhu, Z. Zhong, T. He, and Z. Zhang, "Energy-synchronized computing for sustainable sensor networks," *Ad Hoc Networks*, 2010.

[21] H. Yang, and Y. Zhang, "Analysis of Supercapacitor Energy Loss for Power Management in Environmentally Powered Wireless Sensor Nodes," *IEEE Transaction on Power Electronics*, vol.28, no.11, pp.5391-5403, 2013.

[22] G.V. Merrett, and A.S. Weddell, "Supercapacitor leakage in energy-harvesting sensor nodes: Fact or fiction?" *2012 Ninth International Conference on Networked Sensing Systems (INSS)*, pp.1-5, 2012.

[23] Y. Zhang, and H. Yang, "Modeling and characterization of supercapacitors for wireless sensor network applications," *Journal of Power Sources*, vol.196, no.8 , pp.4128-4135, 2011.

[24] H. Yang, and Y. Zhang, "Self-discharge analysis and characterization of supercapacitors for environmentally powered wireless sensor network applications," *Journal of Power Sources*, vol.196, no.20, pp.8866-8873, 2011.

[25] Maccor Battery and Cell Test Equipment (Model 4300). Available: http://www.maccor.com/Products/Model4300.aspx.

[26] R. Chai, and Y. Zhang, "A Practical Supercapacitor Model for Power Management in Wireless Sensor Nodes," *IEEE Transactions on Power Electronics*(to be published), 2015.

[27] J. W. Graydon, M. Panjehshahi, and D. W. Kirk, "Charge redistribution and ionic mobility in the micropores of supercapacitors," *Journal of Power Sources*, vol.245, pp.822-829, 2014.

[28] M. Morari and J. Lee, "Model Predictive Control: Past, Present and Future," Computers and Chemical Engineering, vol.23, no.4, pp.667-682, 1999.

[29] C. Renner, J. Jessen, and V. Turau, "Lifetime prediction for supercapacitor-powered wireless sensor nodes," *Proceedings of FGSN*, pp.1-6, 2009.

[30] E.-H. El Brouji, O. Briat, J.-M. Vinassa, *et al.*, "Impact of calendar life and cycling ageing on supercapacitor performance," *IEEE Transactions on Vehicular Technology*, vol.58, no.8, pp.3917-3929, 2009.

[31] Texas Instruments, TPS 61221 - Datasheet, Jan. 2009. [Online]. Available: http://focus.ti.com/lit/ds/symlink/tps61221.pdf.

[32] C. Renner, F. Meier, and V. Turau, "Holistic online energy assessment: Feasibility and practical application," *2012 Ninth International Conference on Networked Sensing Systems (INSS)*, 2012.

[33] J. Polastre, R. Szewczyk, and D. Culler, "Telos: enabling ultra-low power wireless research," *IEEE International Symposium on Information Processing in Sensor Networks (IPSN)*, 2005.